Published December 16, 2013

Spindle assembly checkpoint robustness requires Tpr-mediated regulation of Mad1/Mad2 proteostasis

Nina Schweizer,[1] Cristina Ferrás,[1] David M. Kern,[3,4] Elsa Logarinho,[1,2] Iain M. Cheeseman,[3,4] and Helder Maiato[1,2]

[1]Chromosome Instability and Dynamics Laboratory, Instituto de Biologia Molecular e Celular, and [2]Cell Division Unit, Department of Experimental Biology, Faculdade de Medicina, Universidade do Porto, 4099-002 Porto, Portugal
[3]Whitehead Institute for Biomedical Research and [4]Department of Biology, Massachusetts Institute of Technology, Cambridge, MA 02142

Tpr is a conserved nuclear pore complex (NPC) protein implicated in the spindle assembly checkpoint (SAC) by an unknown mechanism. Here, we show that Tpr is required for normal SAC response by stabilizing Mad1 and Mad2 before mitosis. Tpr coimmunoprecipitated with Mad1 and Mad2 (hereafter designated as Tpr/Mad1/Mad2 or TM2 complex) during interphase and mitosis, and is required for Mad1–c-Mad2 recruitment to NPCs. Interestingly, Tpr was normally undetectable at kinetochores and dispensable for Mad1, but not for Mad2, kinetochore localization, which suggests that SAC robustness depends on Mad2 levels at kinetochores. Protein half-life measurements demonstrate that Tpr stabilizes Mad1 and Mad2, ensuring normal Mad1–c-Mad2 production in an mRNA- and kinetochore-independent manner. Overexpression of GFP-Mad2 restored normal SAC response and Mad2 kinetochore levels in Tpr-depleted cells. Mechanistically, we provide evidence that Tpr might spatially regulate SAC proteostasis through the SUMO-isopeptidases SENP1 and SENP2 at NPCs. Thus, Tpr is a kinetochore-independent, rate-limiting factor required to mount and sustain a robust SAC response.

Introduction

The spindle assembly checkpoint (SAC) ensures correct chromosome segregation by providing time for proper kinetochore (KT) attachment to spindle microtubules (MTs) through inhibition of the anaphase-promoting complex (APC; Musacchio and Salmon, 2007). Critical to this inhibition is the repression of the APC activator Cdc20 by Mad2, thereby preventing premature degradation of cyclin B and securin. Mad2 exists in two distinct pools at KTs: one that is stable and another with high turnover (Shah et al., 2004; Vink et al., 2006). The stable pool of Mad2 is bound to Mad1, adopting a structural conformation known as closed-Mad2 (c-Mad2; Sironi et al., 2002; Luo et al., 2004; De Antoni et al., 2005; Mapelli et al., 2007). The Mad1–c-Mad2 complex at unattached KTs acts as a receptor for an inactive cytosolic open-Mad2 (o-Mad2) conformer that is converted into active c-Mad2 by binding to this template. c-Mad2 is selectively incorporated into the mitotic checkpoint complex (MCC), which is composed of Cdc20, BubR1, and Bub3 and inhibits the APC (Sudakin et al., 2001; Sironi et al., 2002; Luo et al., 2004; Mapelli et al., 2007; Tipton et al., 2011; Chao et al., 2012).

In addition to their localization to KTs, Mad1 and Mad2 are also recruited to the nuclear pore complex (NPC) by the inner nuclear pore protein Tpr, which has been shown to be required for normal SAC response from yeast to humans (Campbell et al., 2001; Ikui et al., 2002; Iouk et al., 2002; Scott et al., 2005; Lee et al., 2008; De Souza et al., 2009; Lince-Faria et al., 2009; Ding et al., 2012). However, the underlying molecular mechanism remains unclear. Here, we dissect how human Tpr regulates the SAC response and propose a mechanism by which Tpr association with Mad1 and Mad2 ensures proper SAC proteostasis throughout the cell cycle that is required to mount and sustain a robust SAC response.

N. Schweizer and C. Ferrás contributed equally to this paper.

Correspondence to Helder Maiato: maiato@ibmc.up.pt

Abbreviations used in this paper: ACA, anticentromere antibody; APC, anaphase-promoting complex; CCD, charge-coupled device; IP, immunoprecipitation; KT, kinetochore; LAP, local affinity purification; MCC, mitotic checkpoint complex; MT, microtubule; NEB, nuclear envelope breakdown; NPC, nuclear pore complex; PLA, proximity ligation assay; ROI, region of interest; SAC, spindle assembly checkpoint; WB, Western blot.

Supplemental Material can be found at:
http://jcb.rupress.org/content/suppl/2013/12/15/jcb.201309076.DC1.html

The Rockefeller University Press $30.00
J. Cell Biol. Vol. 203 No. 6 883–893
www.jcb.org/cgi/doi/10.1083/jcb.201309076

Published December 16, 2013

Results and discussion

Tpr is required to sustain a robust SAC response

To determine whether Tpr contributes to SAC robustness, we analyzed mitotic duration using live-cell imaging in control and Tpr-depleted HeLa cells after RNAi, with and without nocodazole (Fig. 1, A–C). Control cells progressed from nuclear envelope breakdown (NEB) to anaphase in 24 ± 5 min, whereas Tpr-depleted cells took 22 ± 5 min (median ± SD, $n = 100$ cells/condition; Fig. 1 B). This difference is statistically significant ($P < 0.01$), especially in the presence of nocodazole (control = 16.5 ± 7.6 h, Tpr RNAi 11.7 ± 7.1 h; median ± SD, $n = 350$ cells/condition, $P < 0.001$; Fig. 1, A and C). Most cells in either experimental condition died after this prolonged mitotic arrest, but cell death occurs significantly earlier in Tpr-depleted cells (control, 15.0 ± 7.0 h; Tpr RNAi, 11.4 ± 6.9 h; median ± SD, $n = 320$ cells/condition, $P < 0.001$; Fig. 1, D and F). A minor fraction of cells undergo mitotic slippage, which also occurs significantly earlier in Tpr-depleted cells (control, 29.2 ± 6.2 h; Tpr RNAi, 13.3 ± 8.8 h; median ± SD, $n = 30$ cells/condition, $P < 0.001$; Fig. 1, E and F). Together, ∼40% of Tpr-depleted cells exit mitosis during the first 10 h of nocodazole treatment, a twofold increase relative to controls (Fig. 1 G).

To confirm the specificity of the phenotype, we performed a rescue experiment using HeLa cells stably expressing an RNAi-resistant mouse Tpr fused to GFP (Fig. 1 H), which interacts with human Mad1 and Mad2 (Hutchins et al., 2010). Tpr-GFP–expressing cells depleted of endogenous Tpr spent equivalent times in mitosis after nocodazole treatment when compared with control HeLa cells (19 ± 5.7 h vs. 16.5 ± 7.6 h; median ± SD, $n = 103$ cells, $P = 0.07$; Fig. 1 I), demonstrating the specificity of the Tpr depletion phenotypes. Thus, Tpr is required for a robust SAC response, supporting previous claims for the existence of intermediate response regimens (Lince-Faria et al., 2009) that cannot be explained by "all-or-nothing" SAC models.

Tpr is required for the localization of a fraction of c-Mad2, but not Mad1, to unattached KTs

We have been unable to detect endogenous or GFP-tagged Tpr at KTs by fluorescence microscopy (Lince-Faria et al., 2009; and unpublished data). Previous studies also reported conflicting findings regarding the effect of Tpr depletion on the KT localization of the SAC proteins Mad1 and Mad2 (Lee et al., 2008; Lince-Faria et al., 2009). To clarify this, we performed quantitative immunofluorescence microscopy with specific antibodies against Cdc20, BubR1, Mad1, and total Mad2 (t-Mad2), as well as the c-Mad2 (Fava et al., 2011) and o-Mad2 (Hewitt et al., 2010) conformers, in nocodazole-treated control and Tpr-depleted cells (Fig. 2 A). After Tpr RNAi, t-Mad2 levels at KTs decrease by ∼50%, with equivalent reductions in the levels of c-Mad2 and o-Mad2 (Fig. 2 B). In contrast, Mad1 levels at KTs increase by ∼40%, whereas Cdc20 and BubR1 increase by ∼80% (Fig. 2 B), which might reflect a feedback response caused by an effective reduction of cytosolic MCC. This would be consistent with previous work in yeast that showed that alteration of the normal Mad1/Mad2 ratio compromises SAC response (Barnhart et al., 2011). Importantly, c-Mad2 levels at unattached KTs are also reduced after Tpr depletion using a distinct siRNA target sequence (Rajanala and Nandicoori, 2012) and are restored by expression of RNAi-resistant mouse Tpr-GFP (Figs. 2 B and S1, A–D), ruling out possible Mad2 off-targeting effects. Altogether, these results indicate that normal localization of c-Mad2 and o-Mad2 to unattached KTs is compromised after Tpr depletion.

The reduction of o-Mad2 at KTs in Tpr-depleted cells might reflect a proportional reduction of its KT receptor, c-Mad2, or altered turnover at KTs. To distinguish between these possibilities, we performed FRAP analysis of GFP-Mad2 at KTs in control and Tpr-depleted cells treated with nocodazole. In both conditions, GFP-Mad2 displays indistinguishable, rapid recovery with single exponential kinetics (control, $t_{1/2} = 6 \pm 8$ s, $n = 10$ KTs; Tpr RNAi, $t_{1/2} = 4 \pm 3$ s, $n = 8$ KTs; median ± SD, $P = 0.22$) with a similar extent of recovery (control, 58 ± 18%, $n = 10$ KTs; Tpr RNAi, 57 ± 14%, $n = 8$ KTs; median ± SD, $P = 0.22$; Fig. 2 C). These findings demonstrate that Tpr does not impact Mad2 dynamics at unattached KTs, which suggests that Tpr promotes the localization of c-Mad2 to unattached KTs and is rate-limiting for the conversion of o-Mad2 into cytoplasmic c-Mad2.

Tpr interacts with Mad1 and Mad2 throughout the cell cycle

Tpr interacts with Mad1 and Mad2 (Lee et al., 2008; Lince-Faria et al., 2009). To investigate the nature of these interactions, we isolated GFP-Mad1 from nocodazole-arrested mitotic cells using a cross-linking strategy and mass spectrometry. In parallel, we performed coimmunoprecipitation (co-IP) experiments with endogenous Mad1 in asynchronous or mitotic enriched populations (Fig. 3 B). We found that Mad1 associates with Tpr, cyclin B/Cdk1, and Mad2, but failed to detect Cdc20, BubR1, or Bub3 (Fig. 3, A and B), which suggests that the TM2 complex exists independently of the MCC throughout the cell cycle. Importantly, IP of a GFP-Mad1 mutant (KVLHM-5A) that is unable to interact with Mad2 (Kim et al., 2012) also isolated Tpr, which suggests that Tpr interaction with Mad1 is independent of Mad2 (Fig. 3 A). To test where these proteins interact, we performed an in situ proximity ligation assay (PLA; Söderberg et al., 2006). This revealed abundant fluorescent PLA foci between Tpr and Mad1 at the nuclear periphery, likely corresponding to NPCs (Fig. 3, C and D). Tpr depletion by RNAi or a PLA reaction between the core nuclear pore protein Nup107 and Mad1 abolished the formation of fluorescent foci (Fig. 3, C and D). No Tpr/Mad1 PLA foci were ever detected at unattached KTs in cells treated with nocodazole (Fig. 3 C). These findings, together with our IP experiments, strongly suggest that Tpr interacts with Mad1 at the nuclear envelope during interphase, but not at KTs during mitosis. Consistent with this conclusion, Tpr depletion disrupted the localization of both Mad1 and c-Mad2 at NPCs during interphase (Fig. 3 E).

Published December 16, 2013

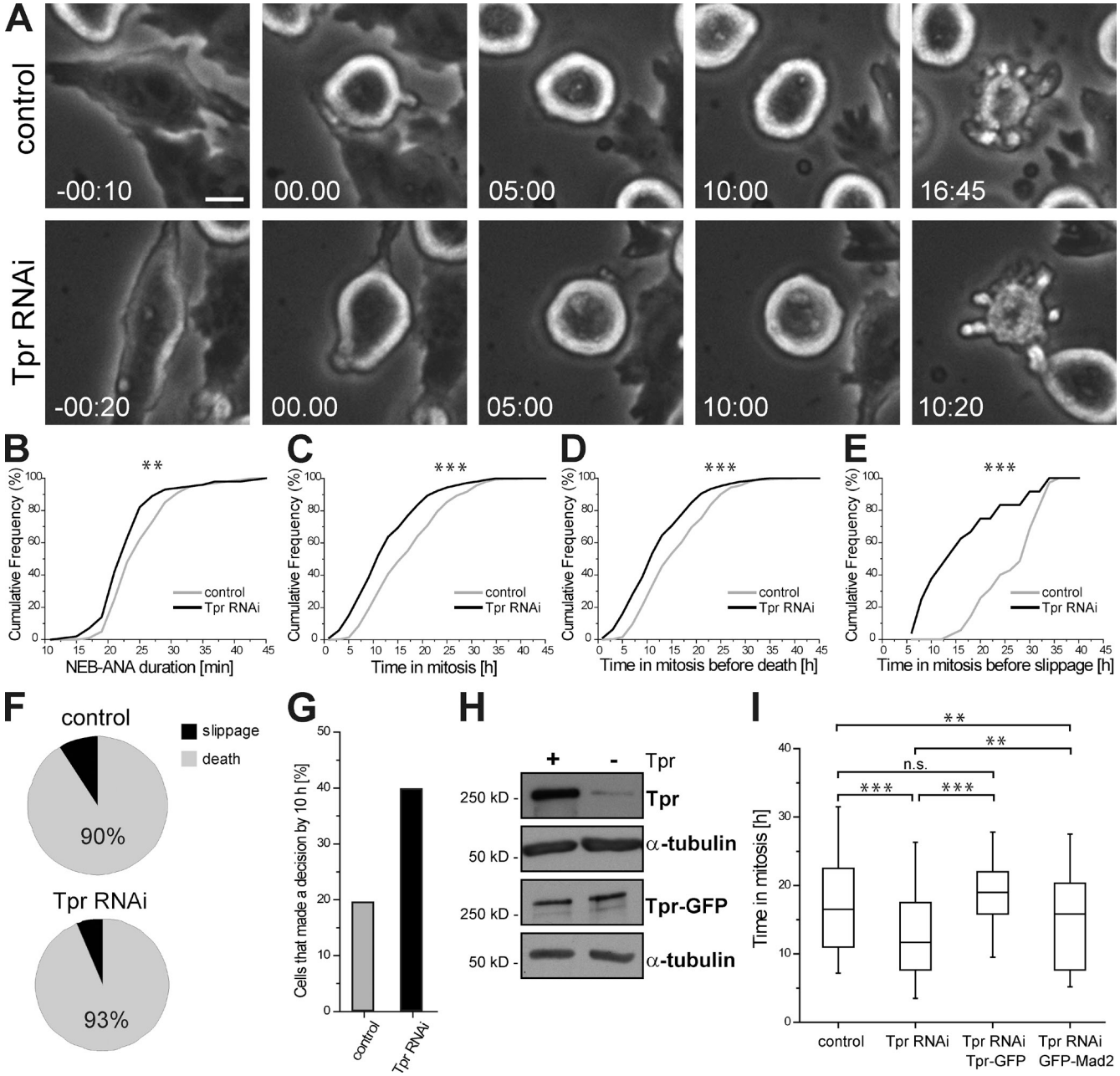

Figure 1. **Tpr is required for a robust SAC response.** (A) Live cell analysis of control and Tpr-depleted HeLa cells after nocodazole treatment. Bar, 10 µm. (B) Tpr depletion reduces the time from NEB to anaphase (ANA) onset. The data shown are from a single representative experiment (control, 24 ± 5 min, n = 100 cells; Tpr RNAi, 22 ± 5 min, n = 100 cells; median ± SD, $P < 0.05$) out of two independent experiments. (C) Tpr-depleted cells spend less time in mitosis when challenged with nocodazole. The data shown are from a single representative experiment (control, 16.5 ± 7.6 h, n = 350 cells; Tpr RNAi, 11.7 ± 7.1 h, n = 360 cells; median ± SD, $P < 0.001$) out of two independent experiments. (D and F) Most control and Tpr-depleted cells die after a prolonged mitotic arrest, but death occurs earlier after Tpr RNAi. The data shown are from a single representative experiment (control, 15 ± 7 h, n = 315 cells; Tpr RNAi, 11 ± 6.9 h, n = 336 cells; median ± SD, $P < 0.001$) out of two independent experiments. (E) Tpr RNAi cells slip out of mitosis earlier than controls. The data shown are from a single representative experiment (control, 29.2 ± 6.2 h, n = 35 cells; Tpr RNAi, 13.3 ± 8.8 h, n = 24 cells; median ± SD, $P < 0.001$) out of two independent experiments. (G) Twice as many Tpr-depleted cells exit mitosis during the first 10 h in nocodazole relative to controls (n = 710 cells from a single representative experiment out of two independent experiments). (H) WB analysis of Tpr from asynchronous control (+) and Tpr-depleted (−) HeLa cells stably expressing RNAi-resistant Tpr-GFP. α-Tubulin was used as loading control. (I) Time spent in mitosis after nocodazole in control and Tpr-depleted HeLa cells with and without expression of RNAi-resistant Tpr-GFP or GFP-Mad2. Expression of Tpr-GFP rescues mitotic timing. The data shown are from a single representative experiment (19 ± 5.7 h, n = 103 cells; median ± SD, $P > 0.05$). Cells overexpressing Mad2 spent slightly less time in mitosis. The data shown are from a single representative experiment (15.8 ± 7.6 h, n = 115 cells; median ± SD, $P < 0.05$). Boxes represent interquartile distributions and whiskers represent 5th and 95th percentiles. n.s., not significant. **, $P < 0.01$; ***, $P < 0.001$.

Tpr is rate-limiting for the amount of Mad1–c-Mad2 produced before mitosis

The previous data raised the possibility that Tpr may function as a scaffold for regulating the assembly or stability of Mad1–c-Mad2 before their targeting to KTs. To test this hypothesis, we performed IP experiments to investigate the amount of Mad1–c-Mad2 produced in asynchronous and mitotic extracts. We found that Tpr depletion results in ∼50%

Published December 16, 2013

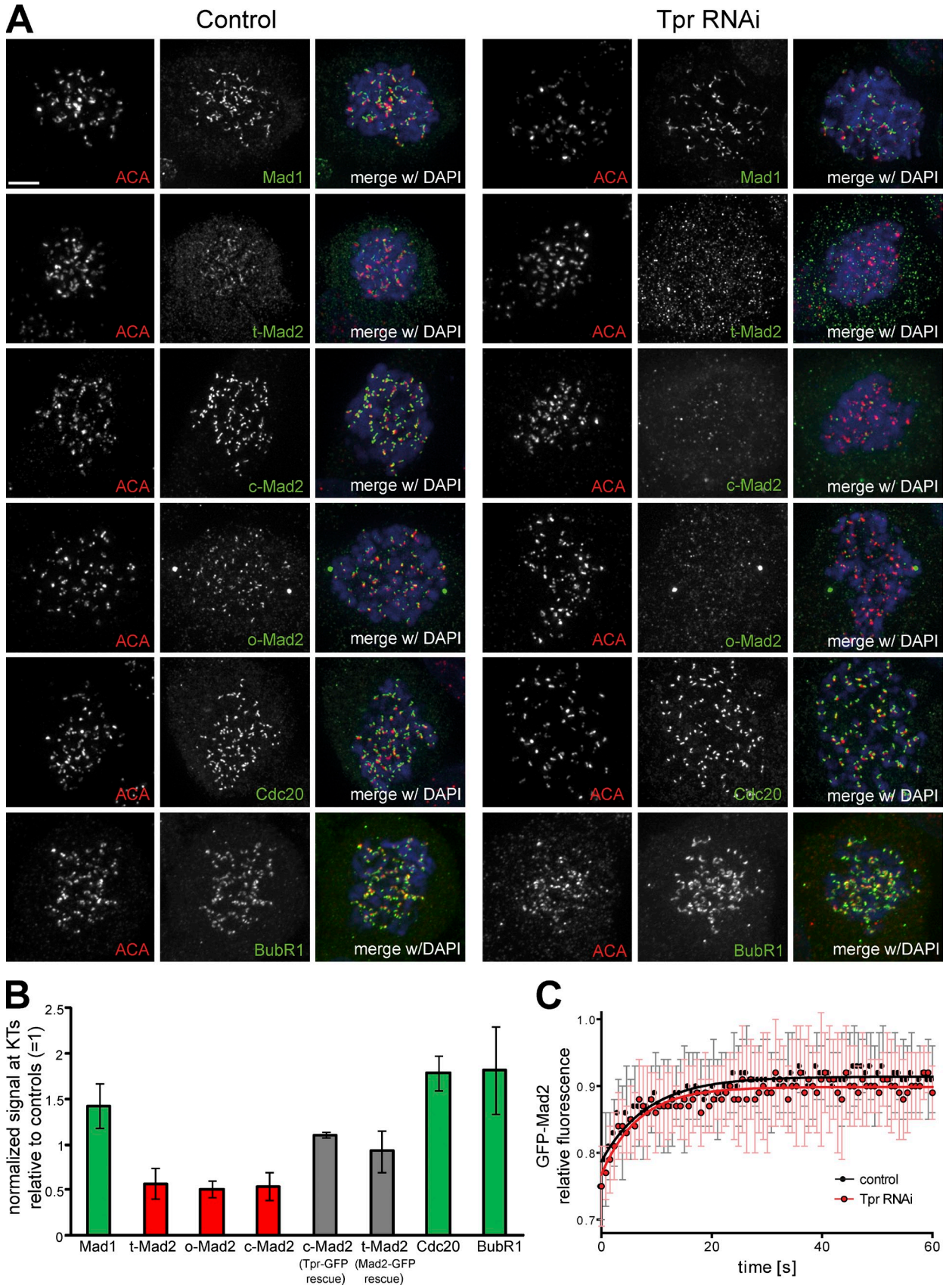

Figure 2. **Tpr is required for c-Mad2, but not Mad1, localization at unattached KTs.** (A) Immunofluorescence of nocodazole-treated control and Tpr-depleted HeLa cells with the indicated antibodies. Bar, 5 µm. (B) Normalized fluorescence signals at KTs from Tpr-depleted cells relative to controls (set to 1). Error bars represent standard deviations from the mean obtained from two or three independent experiments. Green and red boxes correspond to parental HeLa cells.

Published December 16, 2013

A

IP	% Seq Coverage	# Peptides	MW (kD)
Mad1	71	1127	83.1
Mad2	10.2	3	23.5
Tpr	6.9	18	267.3
Cyclin B	5.8	4	48.3
Cdk1	29	13	34.1
Mad1(KVLHM-5A)	60.2	63	83.1
Tpr	19.8	41	267.3
Cdk1	23.2	5	34.1

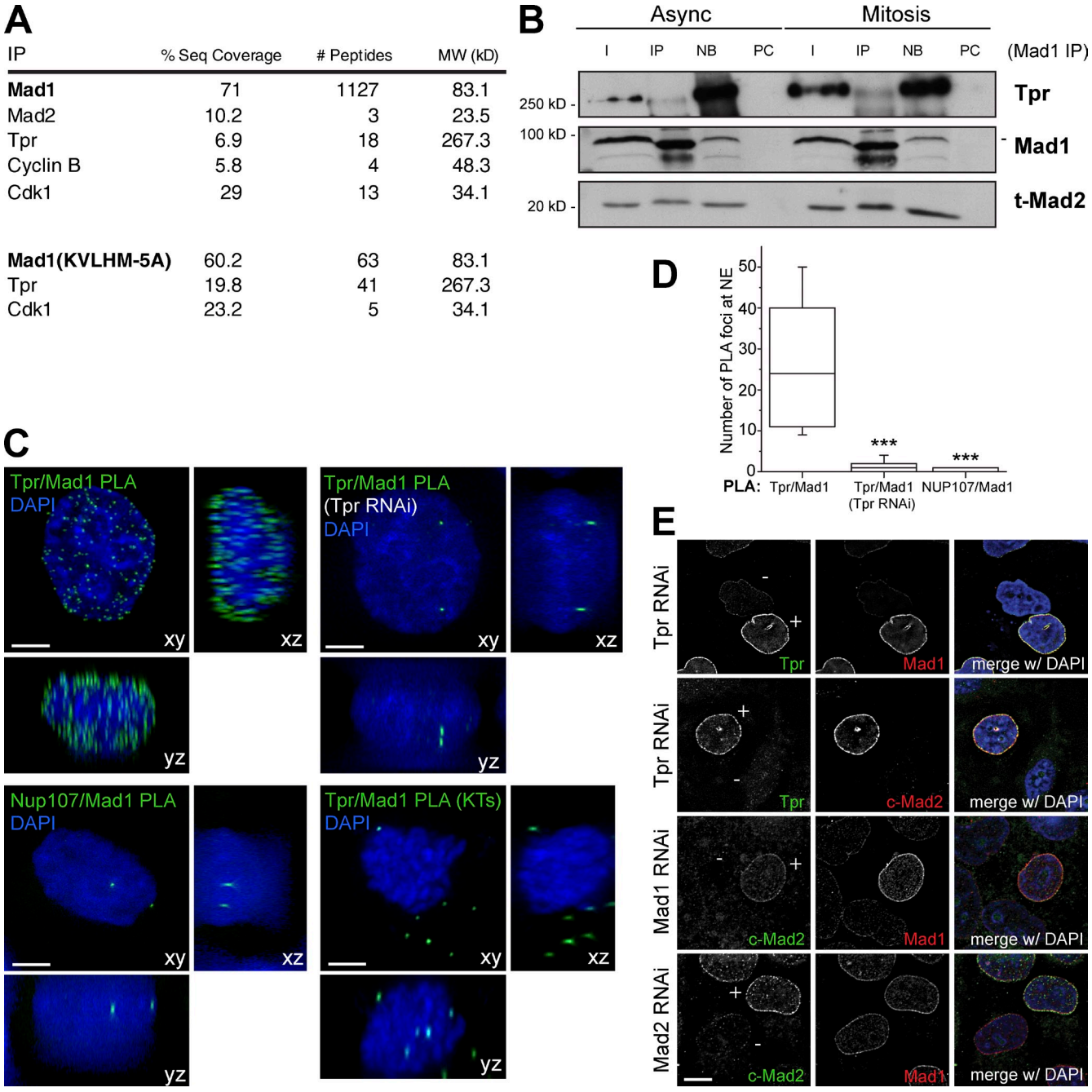

Figure 3. **Tpr interacts with Mad1 and Mad2 throughout the cell cycle.** (A) LAP-Mad1 purification followed by mass spectrometry analysis reveals interactions with Mad2, Cyclin B, Cdk1, and Tpr during mitosis. A Mad1 mutant (KVLHM-5A) that does not bind Mad2 is still able to interact with Tpr. (B) IP from asynchronous (Async) and mitotic HeLa cells (Mitosis) using a Mad1 antibody. I, input; PC, pre clear; IP, immunoprecipitated; NB, nonbinding fraction. All fractions were analyzed by WB for detection of Tpr, Mad1, and t-Mad2. (C) 3D image projections from PLA experiments between Tpr and Mad1 at NPCs in interphase and unattached KTs in mitotic HeLa cells treated with nocodazole. Green foci indicate a positive reaction, and nuclei/chromosomes were counterstained with DAPI. PLA between Nup107 and Mad1, as well as between Tpr and Mad1 upon Tpr RNAi were used as negative controls. Bars, 5 µm. (D) Quantification of the PLA foci at the nuclear envelope (NE) for Tpr/Mad1, Nup107/Mad1, and Tpr/Mad1 upon Tpr RNAi in interphase. Error bars represent standard deviations from three independent experiments. (E) Immunofluorescence with Tpr, Mad1, and c-Mad2 antibodies. Tpr depletion prevented Mad1 and c-Mad2 localization at the nuclear envelope. + and − signs indicate nondepleted and depleted cells, respectively. Bar, 10 µm.

reduction of Mad1 and Mad2 that co-IP in both asynchronous and mitotic populations (Fig. 4, A and B). Importantly, we found that the starting amount of Mad1 and Mad2 present in the extracts (input) proportionally decreases after Tpr depletion (Fig. 4, A and B), which suggests that Tpr affects the cellular pool of Mad1 and Mad2.

Gray boxes correspond to HeLa cells stably expressing Tpr-GFP or GFP-Mad2. (C) FRAP of GFP-Mad2 in control and Tpr-depleted HeLa cells. Data points represent means obtained from 10 (control) or 8 (Tpr RNAi) KTs, to which a single exponential curve was fit. Error bars represent standard deviation.

Published December 16, 2013

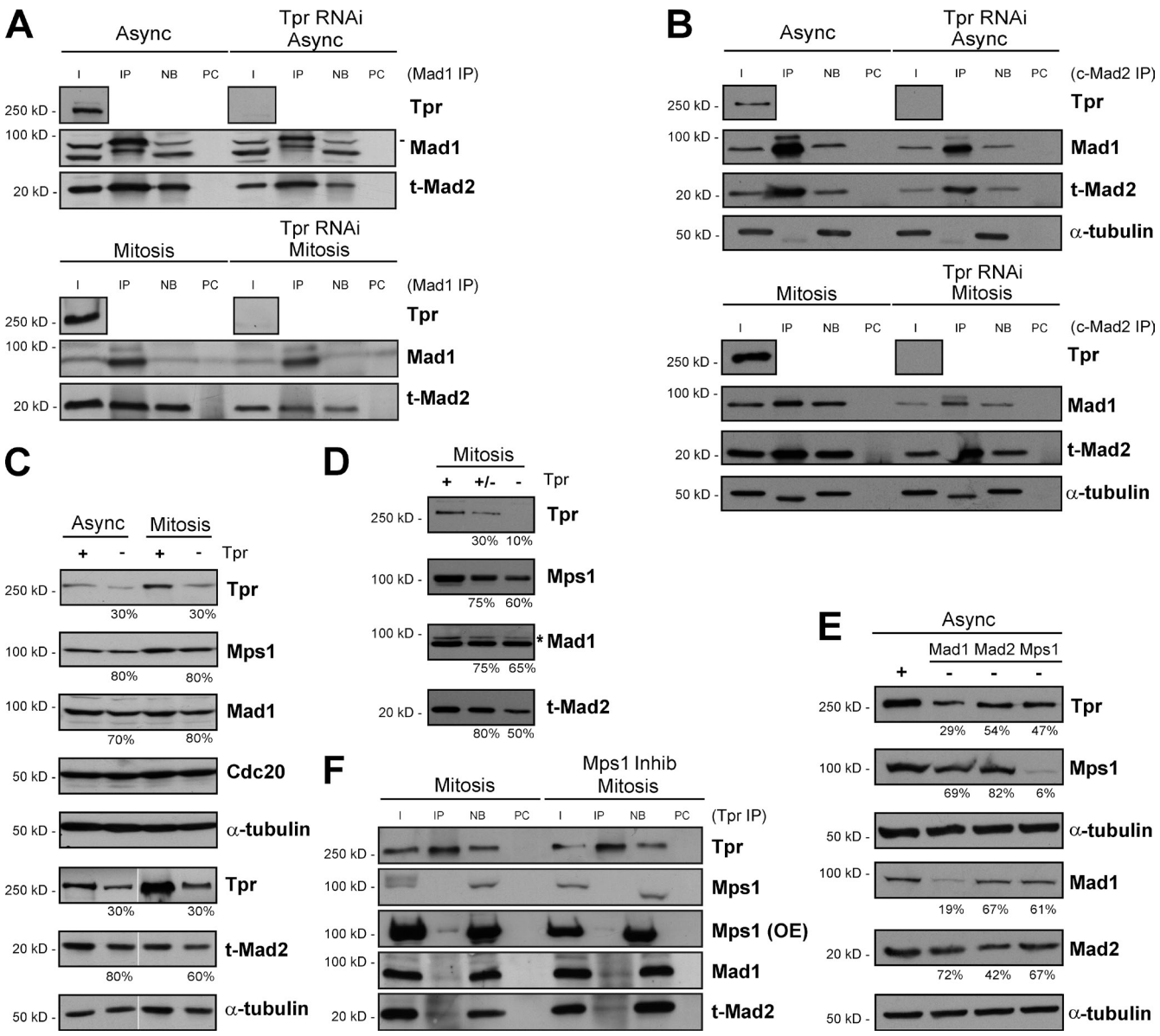

Figure 4. **Tpr regulates the available amount of Mad1–c-Mad2.** (A) IP of Mad1 from asynchronous (Async) and mitotic (Mitosis) HeLa cells with or without Tpr. (B) IP of c-Mad2 from asynchronous and mitotic HeLa cells with or without Tpr. Note the decrease of coimmunoprecipitated Mad1–c-Mad2 after Tpr RNAi. (C) WB analysis of asynchronous and mitotic HeLa cell extracts from control and Tpr-depleted cells to detect the indicated proteins. Note the reduction of Mps1, Mad1, and Mad2 after Tpr RNAi indicated by the respective percentage relative to controls. (D) WB analysis of mitotic HeLa cells to detect the indicated proteins after different extents of Tpr depletion. The asterisk indicates the quantified band. (E) WB analysis of Tpr, Mad1, Mad2, and Mps1 upon partial depletion of Mad1, Mad2, or Mps1 by RNAi. + and – signs indicate control and depleted cells, respectively. (F) IP from mitotic HeLa cells with or without Mps1 inhibition using a Tpr antibody followed by WB against Tpr, Mps1, Mad1, and t-Mad2. α-Tubulin was used as loading control in all experiments. OE, overexposed.

To test whether Tpr is required for the expression or stability of SAC-related proteins, we performed a semiquantitative Western blot (WB) analysis using asynchronous and mitotic extracts derived from control and Tpr-depleted cells. We found that the protein levels of Mad1, Mad2, and Mps1, but not Cdc20, decrease after Tpr depletion (Fig. 4 C). Moreover, the observed decrease was proportional to the extent of Tpr depletion (Fig. 4 D). Overall, these data suggest that the interaction between Tpr, Mad1, Mad2, and Mps1 is rate-limiting for the amount of Mad1–c-Mad2 produced before mitosis. In support of this hypothesis, we found that even partial knockdown of Mad1, Mad2, or Mps1 in asynchronous cells decreases the available pool of all the other SAC proteins interacting with Tpr, including Tpr itself (Fig. 4 E).

Tpr associates with Mad1–c-Mad2 independently of KTs and Mps1 kinase activity

Mps1 kinase activity is essential to recruit Mad1–c-Mad2 to unattached KTs (Maciejowski et al., 2010; Santaguida et al., 2010; Sliedrecht et al., 2010; Fig. S2, A–C). Thus, the decrease in Mad2 levels at unattached KTs observed after Tpr RNAi may be a consequence of reduced Mps1 levels or activity. To test these possibilities, we started by partially depleting Mps1

Published December 16, 2013

(Fig. S1 E), and quantified Mad1 and c-Mad2 levels at unattached KTs by fluorescence microscopy. In contrast to the decrease observed in c-Mad2, but not Mad1, after Tpr depletion, we found that both Mad1 and c-Mad2 levels are reduced to a similar extent after partial Mps1 depletion (Fig. S1, F–H). This suggests that the role of Tpr in regulating c-Mad2, but not Mad1, levels at KTs is independent of Mps1. Finally, we determined whether Mps1 kinase activity is required for the interaction between Mad1, Mad2, and Tpr. Based on Tpr IP, Tpr still interacts with Mad1 and Mad2 in mitotic extracts after Mps1 inhibition (Fig. 4 F). Thus, TM2 complex formation is independent of KTs and Mps1 kinase activity.

Tpr is required for SAC proteostasis throughout the cell cycle

It has been proposed that Tpr acts at NPCs as part of a surveillance system that regulates the export of unspliced mRNA into the cytoplasm (Green et al., 2003; Galy et al., 2004; Vinciguerra et al., 2005; Xu et al., 2007; Coyle et al., 2011; Rajanala and Nandicoori, 2012). We tested whether the observed deficit in SAC protein levels reflects a defect in mRNA transcription/processing by quantifying the content of mature mRNA of several SAC genes with real-time PCR. We found similar expression levels for *mad2*, *mps1*, *p31*, and *cdc20* mRNAs in control and Tpr-depleted cells, either in interphase or mitosis (Fig. 5, A and B). Interestingly, *mad1* mRNA expression in interphase is significantly increased ($P < 0.01$) after Tpr depletion (Fig. 5 A), which might reflect a feedback response caused by reduced Mad1 protein levels. Overall, these results demonstrate that the decrease in Mad1, Mad2, and Mps1 after Tpr depletion is not caused by a reduction of the respective mRNAs.

Because Tpr interacts with Mad1, Mad2, and Mps1 and the overall levels of these proteins were reduced upon Tpr depletion, we next investigated a possible role of Tpr in SAC proteostasis by comparing Mad1, Mad2, and Mps1 protein levels in Tpr-depleted extracts derived from asynchronous, G2-enriched, and mitotic cells. In addition, we evaluated whether inhibition of the 26S proteasome by addition of MG132 rescues the effect of Tpr depletion. We found that only asynchronously growing cells partially recover Mad1, Mad2, and Mps1 protein levels after a 2-h treatment with MG132 (Fig. 5 C), which suggests that Tpr regulates the degradation of these proteins before G2 and the commitment to mitosis. Next, we tested whether the observed Mad1, Mad2, and Mps1 degradation after Tpr depletion is responsible for the reduced production of Mad1–c-Mad2 by c-Mad2 IP from control and Tpr-depleted interphase cells in the presence or absence of MG132. We found that Tpr depletion causes a decrease in Mad1 and t-Mad2 present in the extract (input), as well as in the Mad1–c-Mad2 levels. This decrease was partially rescued by incubation with MG132 for 2 h (Fig. 5 D). Finally, we tested whether Tpr is required for the normal turnover of Mad1, Mad2, or Mps1 by treating control and Tpr-depleted cells with cycloheximide to inhibit de novo protein synthesis and monitored the respective protein half-life by WB. We found that Tpr-depleted cells show a significantly shorter half-life for Mad1, Mad2, and, to a lesser extent, Mps1 (Fig. 5, E and F). Based on these experiments, we conclude that Tpr limits the production of Mad1–c-Mad2 by regulating SAC proteostasis.

Overexpression of Mad2 restores Mad2 KT levels and SAC robustness in Tpr-depleted cells

Next, we tested whether the reduced Mad2 protein levels are responsible for the weaker SAC response in Tpr-depleted cells by investigating the ability of Mad2 overexpression to rescue Tpr depletion. For this purpose, we used a cell line expressing ∼1.5× GFP-Mad2 levels relative to endogenous Mad2 (Fig. S1 I). First, we quantified Mad2 levels at unattached KTs in control and Tpr-depleted cells overexpressing GFP-Mad2 by immunofluorescence microscopy upon MT depolymerization with nocodazole (Figs. 2 B and S1 J). We found that GFP-Mad2 overexpression restores t-Mad2 levels at unattached KTs to ∼90% of control levels in Tpr-depleted cells (Fig. 2 B). Next, we quantified the mitotic duration after nocodazole treatment in Tpr-depleted cells overexpressing GFP-Mad2 and found a significant rescue of mitotic duration relative to parental cells depleted of Tpr (15.8 ± 7.6 h vs. 11.7 ± 7.1 h; $n = 115$ cells, $P < 0.01$; Fig. 1 I). We conclude that the proteolytic degradation of Mad2 caused by Tpr depletion is the leading cause of reduced Mad2 levels at unattached KTs and, consequently, of the weaker SAC response.

A mechanism for regulation of SAC proteostasis and robustness by Tpr

Purified Mad1 forms a high-affinity and stable complex with Mad2 in vitro (Sironi et al., 2002; De Antoni et al., 2005), and Mad1 interacts with Mad2 throughout the cell cycle (Chen et al., 1999; Chung and Chen, 2002; Fava et al., 2011). Here we propose that the TM2 complex stabilizes Mad1–c-Mad2 in vivo, preventing it from being degraded by the proteasome. Interestingly, Tpr and respective orthologues in yeast and plants have been implicated in protein SUMOylation at the nuclear periphery, possibly by locally regulating the targeting and/or function of the SUMO-isopeptidases Ulp1/SENP1/SENP2 (Zhao et al., 2004; Xu et al., 2007; David-Watine, 2011). Here we found that Tpr is required to recruit SENP1, but not SENP2, to NPCs (Fig. 5 G). Because Tpr depletion also affects Mad1–c-Mad2 recruitment to NPCs, Mad1–c-Mad2 is not able to interact with either SENP1 or SENP2 at the NPCs, which might alter normal Mad1–c-Mad2 proteostasis. In agreement with this model, either SENP1 or SENP2 depletion by RNAi reduces total Mad1 and Mad2 levels by ∼50% (Fig. 5 H). Given so, it is tempting to speculate that the requirement of Tpr for a robust SAC response by regulating Mad1 and Mad2 protein levels before mitosis might involve spatial control of SUMO-mediated proteolysis at the NPCs, but further studies will be necessary to directly test this hypothesis.

Materials and methods

Cell culture and drug treatments

HeLa or U2OS cells were cultured in DMEM with 10% FBS (Invitrogen) in a 37°C incubator with 5% CO_2 and a humidified atmosphere. MT

Published December 16, 2013

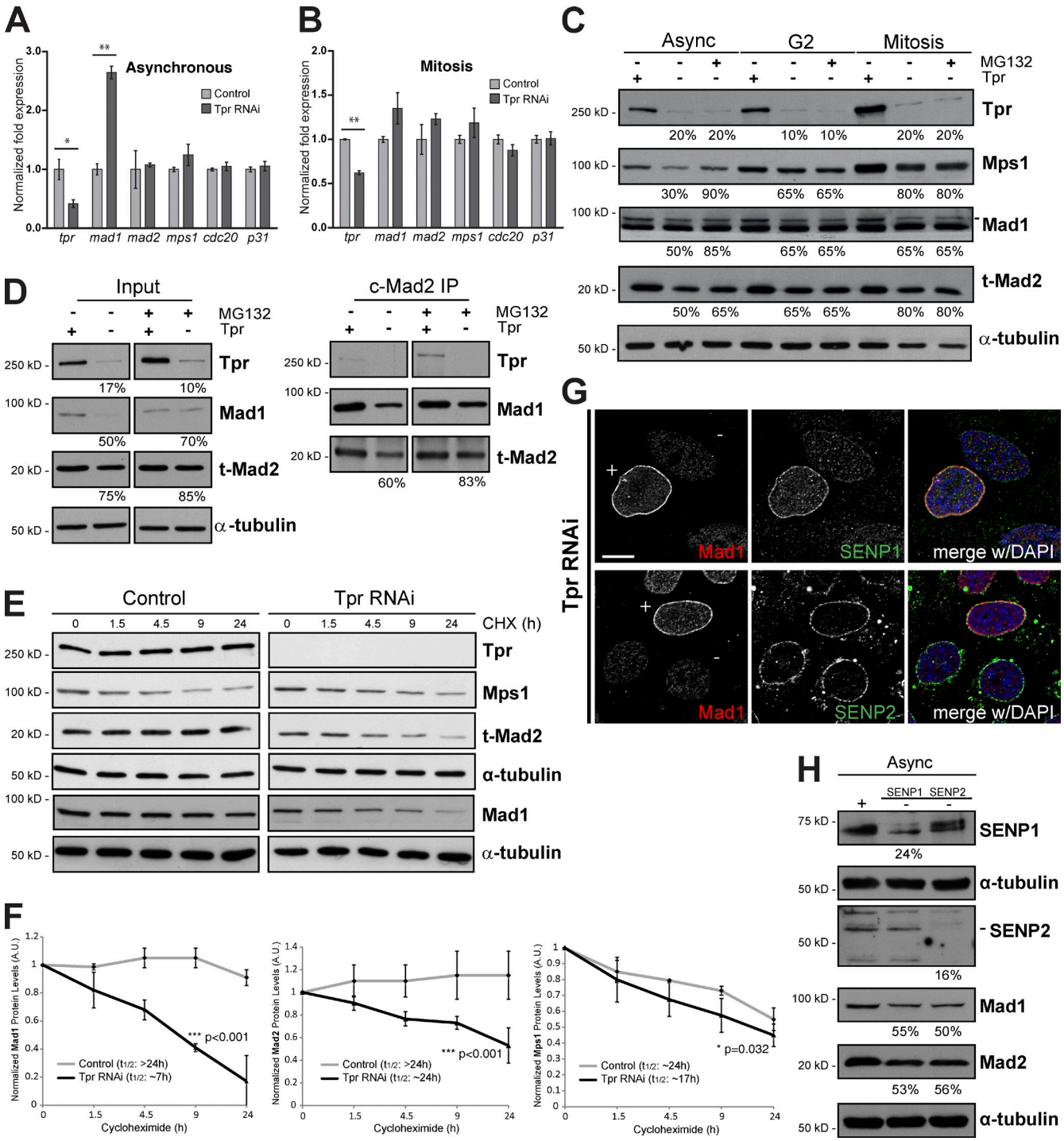

Figure 5. **Tpr is required for SAC proteostasis throughout the cell cycle.** (A and B) Normalized expression of *tpr*, *mad1*, *mad2*, *mps1*, *cdc20*, and *p31* in control and Tpr-depleted asynchronous or mitotic cells. Error bars represent standard deviations from three independent experiments. (C) WB analysis of asynchronous, G2, and mitotic enriched HeLa cell extracts from control (+) and Tpr-depleted (−) cells with (+) or without (−) MG132 with the indicated antibodies. The percentage of protein levels relative to controls is indicated. (D) c-Mad2 IP from asynchronous and mitotic HeLa cells with (+) or without (−) Tpr, in the presence (+) or absence (−) of MG132. (E and F) Cells with or without Tpr were treated with cycloheximide (CHX) for various time points as indicated. Total protein extracts of asynchronous HeLa cells were analyzed by WB to detect Tpr, Mps1, Mad1, and t-Mad2 in control and Tpr-depleted cells. α-Tubulin was used as a loading control. *, $P < 0.05$; **, $P < 0.01$; ***, $P < 0.001$. The error bars indicate standard deviations from two independent experiments. (G) Immunodetection of Mad1 (red), SENP1, and SENP2 (green) in Tpr-depleted cells (−). A nondepleted cell (+) was used as internal control. DNA was counterstained with DAPI (blue). (H) WB analysis of asynchronous cell extracts in control and after SENP1 or SENP2 RNAi. The percentage of protein levels relative to controls is indicated. α-Tubulin was used as a loading control. Bar, 10 µm.

Published December 16, 2013

depolymerization in HeLa and U2OS cells was induced by nocodazole at 1.6 µM for 2–16 h, according to the experiment. To inhibit the proteasome, induce a metaphase arrest, and prevent exit due to a compromised SAC, cells were treated with 5 µM MG132 (EMD Millipore) for 2 h. For Mps1 inhibition, cells were treated with 10 µM Mps1-IN-1 (provided by N. Gray) for 1 h. Mis12-Mps1 expression was induced with 1 µg/ml doxycycline (Sigma-Aldrich) for 24 h. G2-enriched extracts were derived from cells incubated for 16 h with the Cdk1 inhibitor RO3306 (Roche), whereas mitotic extracts were obtained by shake-off upon nocodazole treatment for 16 h. For determination of protein half-life, HeLa cells were exposed to 10 µg/ml cycloheximide (Sigma-Aldrich) in growth medium, both in the presence or absence of Tpr. Cells were incubated at 37°C with 5% CO_2 for different time points and subsequently harvested for immunoblotting.

Live cell imaging

Control and Tpr-depleted cells (parental HeLa cells and HeLa cells stably expressing GFP-Mad2 or Tpr-GFP) were imaged with phase-contrast microscopy at 37°C in DMEM or L15 medium (Invitrogen) supplemented with 10% FBS. To determine the time between NEB and anaphase onset, images were captured on an inverted microscope (TE2000U; Nikon; 20× objective lens; LWD; 0.4 NA) equipped with an electron-multiplying charge-coupled device (CCD) camera (iXonEM+; Andor Technology) every 2 min for 12 h using the NIS-Elements Viewer software (Nikon). To measure mitotic timing and to determine the cell fate after interfering with MTs, nocodazole was added 1 h after filming, and images were acquired on an inverted microscope (Axiovert 200M; Carl Zeiss; 20× objective lens; A-Plan Ph1; 0.3 NA) equipped with a CCD camera (CoolSNAP HQ2; Photometrics) every 10 min for 48 h using the Micro-Manager 1.3 software (www.micro-manager.org).

Immunofluorescence microscopy

Cells were grown on poly-L-lysine–coated coverslips and fixed either with 4% paraformaldehyde or ice-cold methanol, then extracted simultaneously or subsequently with 0.1–0.2% Triton X-100. After short washes in PBS and blocking with 10% FBS in PBS, cells were incubated with primary antibodies after short washes and incubation with the respective secondary antibodies. DNA was counterstained with DAPI (1 µg/ml; Sigma-Aldrich) before coverslips were mounted in 90% glycerol + 10% Tris, pH 8.5, + 0.5% *N*-propyl gallate on glass slides. Images were acquired on a AxioImager Z1 (63× Plan-Apochromatic oil differential interference contrast objective lens, 1.4 NA) equipped with a CCD (Axiocam MR) camera using the Zen software (all from Carl Zeiss) and blind deconvolved using Autoquant X (Media Cybernetics). Images were processed in Photoshop CS4 (Adobe) and represent either maximum projections of a deconvolved stack or a single slice in the case of Figs. 3 E and 5 G. Mouse anti-Mad1 (generated against full-length Mad1, 1:500; provided by A. Santamaria and E. Nigg, Biozentrum, Basel, Switzerland), rabbit anti-Mad1 (generated against full-length Mad1, 1:1,000; provided by P. Meraldi, University of Geneva, Switzerland), mouse anti–c-Mad2 (generated against full-length Mad2, 1:500; provided by A. Santamaria), rabbit anti–t-Mad2 (1:300; Bethyl Laboratories, Inc.), sheep anti–o-Mad2 (generated against full-length Mad2, 1:200; provided by S. Taylor, University of Manchester, UK), rabbit anti-Cdc20 (1:100; Santa Cruz Biotechnology, Inc.), mouse anti-Mps1 (1:100; Merck Millipore), rabbit anti-Tpr (1:500; Novus Biologicals), sheep anti-BubR1 (generated against aa 2–422, 1:300; provided by S. Taylor), rabbit anti-SENP1 or -SENP2 (generated against aa 273–449 and aa 1–92, respectively; 1:1,000; provided by M. Dasso, National Institutes of Health, Bethesda, MD), and human anticentromere antibodies (ACAs; 1:5,000, provided by B. Earnshaw; or 1:2,000, Fitzgerald Industries International) were used as primary antibodies, and Alexa Fluor 488, 568, and 647 (Invitrogen) were used as secondary antibodies (1:1,000).

Fluorescence quantification

For quantification of fluorescence, a custom routine written in MATLAB (MathWorks) was used. Protein accumulation was measured by quantification of pixel gray levels of the focused z plane within a region of interest (ROI). Background fluorescence was measured outside the ROI and subtracted. For quantifications at KTs, the ROI encompassed a single KT or KT pair, and results were normalized against ACA or Mad1 signals. Approximately 1,000 KT pairs from ∼30 cells were analyzed for each protein.

FRAP

FRAP of GFP-Mad2 in control and Tpr RNAi cells treated with nocodazole was performed on an inverted microscope (TE2000U) equipped with an electron-multiplying CCD camera (iXonEM+). Images were acquired every 800 ms. Bleaching in an ROI at a single KT was conducted for 400 ms after three prebleach images were acquired. The fluorescence intensity of the bleached area was normalized using the intensity of an ROI distant to the bleached area (in the same cell) after background subtraction. For calculations of half-time of recovery and percentage of recovery, exponential curve fit was applied to the obtained data using GraphPad Prism 5 (GraphPad Software).

IP and WB

HeLa cells were resuspended in NP-40 lysis buffer (0.5% NP-40). Cell extracts were precleared with protein G magnetic beads (New England Biolabs, Inc.). The cleared lysates were then incubated with the respective antibody. The immunoprecipitates were captured with protein G magnetic beads. The immunoprecipitates were eluted from the beads with SDS sample buffer and subjected to WB analysis. The following antibodies were used for WB: rabbit anti-Tpr antibody (NB100-2866, 1:1,000; Novus Biologicals), mouse anti-Mps1 antibody (NT clone 3-742-1, 1:500; Merck Millipore), rabbit anti-Mad2 antibody (A300-301 A-2, 1:1,000; Bethyl Laboratories, Inc.), rabbit anti-Mad1 antibody (1:1,000; provided by P. Meraldi), mouse anti-Mad1 (1:100; Santa Cruz Biotechnology, Inc.), rabbit anti-Cdc20 antibody (sc-5296, 1:1,000; Santa Cruz Biotechnology, Inc.), rabbit anti-SENP1 or SENP2 (1:2,000), mouse anti-GFP (1:1,000), and mouse anti–α-tubulin antibody (clone B-512, 1:5,000; Sigma-Aldrich). Goat anti–rabbit, anti–mouse, or anti–sheep antibodies were used as secondary antibodies (1:5,000; Jackson ImmunoResearch Laboratories, Inc.). The WBs were quantified using a calibrated densitometer (GS800; Bio-Rad Laboratories) and Quantity One 1-D Analysis Software, version 4.6 (Bio-Rad Laboratories), which highlights saturated pixels when signal intensity falls off the linear range. Only exposures without saturated pixels were used and were normalized for the loading control (α-tubulin).

Local affinity purification (LAP)-Mad1 purification and mass spectrometry

GFP_{LAP} hMad1 was generated in HeLa cells as described previously (Cheeseman et al., 2004). In brief, a pBABE (MMLV)-based plasmid containing GFP_{LAP} hMad1 (or mutant) was cotransfected into 293-GP cells with a VSVG-containing plasmid to generate virus. After infection with the retrovirus, HeLa cells were selected using 2 µg/ml Blasticidin. Resistant cells were sorted by FACS to generate clonal cell lines. To conduct the affinity purifications, cell lines were grown to 70–90% confluency, and then treated with 3.33 µM nocodazole for 16 h. A mitotic shake-off was then performed and cells were pelleted at 1,000 *g*. A modified cross-linking protocol was developed based on Klockenbusch and Kast (2010). In brief, the cell pellets were resuspended with 0.4–1.2% formaldehyde in PBS and rocked gently for 10 min. After pelleting at 1,000 *g*, the cell pellet was quenched with 0.125 M glycine in PBS for 10 min. The cells were processed by sonication and treatment with detergent to solubilize cross-linked cell material, then a one-step LAP purification was performed as described previously (Cheeseman and Desai, 2005) in the presence of 300 mM KCl. In brief, processed lysate was bound to anti-GFP coupled beads for 1 h. The beads were then washed, and bound protein was eluted with 0.1 M glycine. Elutions were TCA-precipitated, and the protein pellet was resuspended with 8 M urea. Cross-linking reversal was performed at 95°C for 5 min before tryptic digestion. Purified proteins were identified by mass spectrometry using an ion trap mass spectrometer (LTQ XL; Thermo Fisher Scientific) with a reverse phase gradient over C18 resin (Phenomenex) and SEQUEST software as described previously (Washburn et al., 2001).

PLA

For PLA, we used primary antibodies raised in different species against Tpr (Novus Biologicals) or Nup107 (provided by V. Doye, Institute Jacques Monod, Paris, France) and Mad1 (provided by A. Santamaria), which were subsequently detected by species-specific secondary antibodies conjugated with PLA probes according to the manufacturer´s instructions (Duolink; Olink Bioscience).

RNA extraction and transcription analysis by RT-qPCR

Total RNA was isolated from interphase, and mitotic HeLa cells (shake-off) were treated with nocodazole and MG132 using an RNeasy Mini kit according to the manufacturer´s instructions (QIAGEN). For cDNA synthesis, 1 µg of total RNA was transcribed with the iScript Select cDNA Synthesis kit (Bio-Rad Laboratories) using the random primers and oligo(dTs) supplied, following the manufacturer's instructions. For each analysis, *gapdh* was used for normalization. RT-qPCRs were performed in the iCycler iQ5 Real-Time PCR Detection System (Bio-Rad Laboratories). The data obtained were analyzed using the Bio-Rad iQ5 Optical System Software v2.1 (Bio-Rad Laboratories).

Published December 16, 2013

Transgenic cell lines

A cell line stably expressing GFP-Mad2 was established by transfecting HeLa cells with a pEGFP-C1-Mad2 plasmid (provided by P. Meraldi) using Fugene HD (Roche). The Tpr-GFP cell line was provided by MitoCheck. The Mis12-Mps1 U2OS cell line was provided by G. Kops (University Medical Center, Utrecht, Netherlands).

RNAi

Depletion of Tpr, Mps1, Mad1, Mad2, SENP1, and SENP2 was performed by transfecting HeLa cells with siRNA oligonucleotides directed against the following target sequences: Tpr, 5′-GGUGGAGAGCGAACAACAG-3′ or 5′-GCACAACAGGAUAAGGUUA-3′; Mps1, 5′-GGUUGAGUUUGUUGCUCAA-3′; Mad1, 5′-CCAAAGUGCUGCACAUGAG-3′; Mad2, 5′-GCGUGGCAUAUAUCCAUCU-3′; SENP1, 5′-UCCUUUACACCUGUCUCGAUGUCUU-3′; and SENP2, 5′-AUAUCUGGAUUCUAUGGGAUU-3′ (all from Sigma-Aldrich), using Lipofectamine RNAiMAX (Invitrogen) according to the manufacturer´s instructions.

Statistical analysis

Statistical analysis was performed using either Graphpad Prism version 5, OriginPro 8 (OriginLab), or SPSS (SPSS advanced statistics 17.0). P-values were calculated with either a Student's *t* test or analysis of variance (ANOVA).

Online supplemental material

Fig. S1 shows experiments in support of the specificity of the Tpr phenotype. Fig. S2 shows the effect of Mps1 inhibition for the loading and maintenance of Mad1–c-Mad2 at unattached KTs. Online supplemental material is available at http://www.jcb.org/cgi/content/full/jcb.201309076/DC1.

We would like to thank Filipe Pinto, Martina Barisic, and Marin Barisic for technical help, and Carolina Lemos for help with statistical analysis. We also thank all colleagues who kindly provided reagents used in this study.

N. Schweizer holds a doctoral fellowship from Fundação para a Ciência e a Tecnologia (FCT) of Portugal (SFRH/BD/69198/2010). Work in the laboratory of H. Maiato is funded by grants PTDC/SAU-ONC/112917/2009 from FCT (COMPETE-FEDER), the Human Frontier Research Program (with I.M. Cheeseman), and the seventh framework program grant PRECISE from the European Research Council.

The authors have no conflicting financial interests.

Author contributions: N. Schweizer and C. Ferrás performed most of the experiments with contributions from I.M. Cheeseman and D.M. Kern. E. Logarinho provided the GFP-Mad2 cell line. N. Schweizer, C. Ferrás, and H. Maiato analyzed the data and wrote the manuscript. H. Maiato designed experiments and coordinated the project.

Submitted: 16 September 2013
Accepted: 11 November 2013

References

Barnhart, E.L., R.K. Dorer, A.W. Murray, and S.C. Schuyler. 2011. Reduced Mad2 expression keeps relaxed kinetochores from arresting budding yeast in mitosis. *Mol. Biol. Cell*. 22:2448–2457. http://dx.doi.org/10.1091/mbc.E09-01-0029

Campbell, M.S., G.K. Chan, and T.J. Yen. 2001. Mitotic checkpoint proteins HsMAD1 and HsMAD2 are associated with nuclear pore complexes in interphase. *J. Cell Sci.* 114:953–963.

Chao, W.C., K. Kulkarni, Z. Zhang, E.H. Kong, and D. Barford. 2012. Structure of the mitotic checkpoint complex. *Nature*. 484:208–213. http://dx.doi.org/10.1038/nature10896

Cheeseman, I.M., and A. Desai. 2005. A combined approach for the localization and tandem affinity purification of protein complexes from metazoans. *Sci. STKE*. 2005:pl1.

Cheeseman, I.M., S. Niessen, S. Anderson, F. Hyndman, J.R. Yates III, K. Oegema, and A. Desai. 2004. A conserved protein network controls assembly of the outer kinetochore and its ability to sustain tension. *Genes Dev.* 18:2255–2268. http://dx.doi.org/10.1101/gad.1234104

Chen, R.H., D.M. Brady, D. Smith, A.W. Murray, and K.G. Hardwick. 1999. The spindle checkpoint of budding yeast depends on a tight complex between the Mad1 and Mad2 proteins. *Mol. Biol. Cell*. 10:2607–2618. http://dx.doi.org/10.1091/mbc.10.8.2607

Chung, E., and R.H. Chen. 2002. Spindle checkpoint requires Mad1-bound and Mad1-free Mad2. *Mol. Biol. Cell*. 13:1501–1511. http://dx.doi.org/10.1091/mbc.02-01-0003

Coyle, J.H., Y.C. Bor, D. Rekosh, and M.L. Hammarskjold. 2011. The Tpr protein regulates export of mRNAs with retained introns that traffic through the Nxf1 pathway. *RNA*. 17:1344–1356. http://dx.doi.org/10.1261/rna.2616111

David-Watine, B. 2011. Silencing nuclear pore protein Tpr elicits a senescent-like phenotype in cancer cells. *PLoS ONE*. 6:e22423. http://dx.doi.org/10.1371/journal.pone.0022423

De Antoni, A., C.G. Pearson, D. Cimini, J.C. Canman, V. Sala, L. Nezi, M. Mapelli, L. Sironi, M. Faretta, E.D. Salmon, and A. Musacchio. 2005. The Mad1/Mad2 complex as a template for Mad2 activation in the spindle assembly checkpoint. *Curr. Biol.* 15:214–225. http://dx.doi.org/10.1016/j.cub.2005.01.038

De Souza, C.P., S.B. Hashmi, T. Nayak, B. Oakley, and S.A. Osmani. 2009. Mlp1 acts as a mitotic scaffold to spatially regulate spindle assembly checkpoint proteins in *Aspergillus nidulans*. *Mol. Biol. Cell*. 20:2146–2159. http://dx.doi.org/10.1091/mbc.E08-08-0878

Ding, D., S. Muthuswamy, and I. Meier. 2012. Functional interaction between the Arabidopsis orthologs of spindle assembly checkpoint proteins MAD1 and MAD2 and the nucleoporin NUA. *Plant Mol. Biol.* 79:203–216. http://dx.doi.org/10.1007/s11103-012-9903-4

Fava, L.L., M. Kaulich, E.A. Nigg, and A. Santamaria. 2011. Probing the in vivo function of Mad1:C-Mad2 in the spindle assembly checkpoint. *EMBO J.* 30:3322–3336. http://dx.doi.org/10.1038/emboj.2011.239

Galy, V., O. Gadal, M. Fromont-Racine, A. Romano, A. Jacquier, and U. Nehrbass. 2004. Nuclear retention of unspliced mRNAs in yeast is mediated by perinuclear Mlp1. *Cell*. 116:63–73. http://dx.doi.org/10.1016/S0092-8674(03)01026-2

Green, D.M., C.P. Johnson, H. Hagan, and A.H. Corbett. 2003. The C-terminal domain of myosin-like protein 1 (Mlp1p) is a docking site for heterogeneous nuclear ribonucleoproteins that are required for mRNA export. *Proc. Natl. Acad. Sci. USA*. 100:1010–1015. http://dx.doi.org/10.1073/pnas.0336594100

Hewitt, L., A. Tighe, S. Santaguida, A.M. White, C.D. Jones, A. Musacchio, S. Green, and S.S. Taylor. 2010. Sustained Mps1 activity is required in mitosis to recruit O-Mad2 to the Mad1-C-Mad2 core complex. *J. Cell Biol.* 190:25–34. http://dx.doi.org/10.1083/jcb.201002133

Hutchins, J.R., Y. Toyoda, B. Hegemann, I. Poser, J.K. Hériché, M.M. Sykora, M. Augsburg, O. Hudecz, B.A. Buschhorn, J. Bulkescher, et al. 2010. Systematic analysis of human protein complexes identifies chromosome segregation proteins. *Science*. 328:593–599. http://dx.doi.org/10.1126/science.1181348

Ikui, A.E., K. Furuya, M. Yanagida, and T. Matsumoto. 2002. Control of localization of a spindle checkpoint protein, Mad2, in fission yeast. *J. Cell Sci.* 115:1603–1610.

Iouk, T., O. Kerscher, R.J. Scott, M.A. Basrai, and R.W. Wozniak. 2002. The yeast nuclear pore complex functionally interacts with components of the spindle assembly checkpoint. *J. Cell Biol.* 159:807–819. http://dx.doi.org/10.1083/jcb.200205068

Kim, S., H. Sun, D.R. Tomchick, H. Yu, and X. Luo. 2012. Structure of human Mad1 C-terminal domain reveals its involvement in kinetochore targeting. *Proc. Natl. Acad. Sci. USA*. 109:6549–6554. http://dx.doi.org/10.1073/pnas.1118210109

Klockenbusch, C., and J. Kast. 2010. Optimization of formaldehyde cross-linking for protein interaction analysis of non-tagged integrin beta1. *J. Biomed. Biotechnol.* 2010:927585. http://dx.doi.org/10.1155/2010/927585

Lee, S.H., H. Sterling, A. Burlingame, and F. McCormick. 2008. Tpr directly binds to Mad1 and Mad2 and is important for the Mad1-Mad2-mediated mitotic spindle checkpoint. *Genes Dev.* 22:2926–2931. http://dx.doi.org/10.1101/gad.1677208

Lince-Faria, M., S. Maffini, B. Orr, Y. Ding, Cláudia Florindo, C.E. Sunkel, A. Tavares, J. Johansen, K.M. Johansen, and H. Maiato. 2009. Spatiotemporal control of mitosis by the conserved spindle matrix protein Megator. *J. Cell Biol.* 184:647–657. http://dx.doi.org/10.1083/jcb.200811012

Luo, X., Z. Tang, G. Xia, K. Wassmann, T. Matsumoto, J. Rizo, and H. Yu. 2004. The Mad2 spindle checkpoint protein has two distinct natively folded states. *Nat. Struct. Mol. Biol.* 11:338–345. http://dx.doi.org/10.1038/nsmb748

Maciejowski, J., K.A. George, M.E. Terret, C. Zhang, K.M. Shokat, and P.V. Jallepalli. 2010. Mps1 directs the assembly of Cdc20 inhibitory complexes during interphase and mitosis to control M phase timing and spindle checkpoint signaling. *J. Cell Biol.* 190:89–100. http://dx.doi.org/10.1083/jcb.201001050

Mapelli, M., L. Massimiliano, S. Santaguida, and A. Musacchio. 2007. The Mad2 conformational dimer: structure and implications for the spindle

assembly checkpoint. *Cell*. 131:730–743. http://dx.doi.org/10.1016/j.cell.2007.08.049

Musacchio, A., and E.D. Salmon. 2007. The spindle-assembly checkpoint in space and time. *Nat. Rev. Mol. Cell Biol.* 8:379–393. http://dx.doi.org/10.1038/nrm2163

Rajanala, K., and V.K. Nandicoori. 2012. Localization of nucleoporin Tpr to the nuclear pore complex is essential for Tpr mediated regulation of the export of unspliced RNA. *PLoS ONE*. 7:e29921. http://dx.doi.org/10.1371/journal.pone.0029921

Santaguida, S., A. Tighe, A.M. D'Alise, S.S. Taylor, and A. Musacchio. 2010. Dissecting the role of MPS1 in chromosome biorientation and the spindle checkpoint through the small molecule inhibitor reversine. *J. Cell Biol.* 190:73–87. http://dx.doi.org/10.1083/jcb.201001036

Scott, R.J., C.P. Lusk, D.J. Dilworth, J.D. Aitchison, and R.W. Wozniak. 2005. Interactions between Mad1p and the nuclear transport machinery in the yeast *Saccharomyces cerevisiae*. *Mol. Biol. Cell*. 16:4362–4374. http://dx.doi.org/10.1091/mbc.E05-01-0011

Shah, J.V., E. Botvinick, Z. Bonday, F. Furnari, M. Berns, and D.W. Cleveland. 2004. Dynamics of centromere and kinetochore proteins; implications for checkpoint signaling and silencing. *Curr. Biol.* 14:942–952.

Sironi, L., M. Mapelli, S. Knapp, A. De Antoni, K.T. Jeang, and A. Musacchio. 2002. Crystal structure of the tetrameric Mad1-Mad2 core complex: implications of a 'safety belt' binding mechanism for the spindle checkpoint. *EMBO J.* 21:2496–2506. http://dx.doi.org/10.1093/emboj/21.10.2496

Sliedrecht, T., C. Zhang, K.M. Shokat, and G.J. Kops. 2010. Chemical genetic inhibition of Mps1 in stable human cell lines reveals novel aspects of Mps1 function in mitosis. *PLoS ONE*. 5:e10251. http://dx.doi.org/10.1371/journal.pone.0010251

Söderberg, O., M. Gullberg, M. Jarvius, K. Ridderstråle, K.J. Leuchowius, J. Jarvius, K. Wester, P. Hydbring, F. Bahram, L.G. Larsson, and U. Landegren. 2006. Direct observation of individual endogenous protein complexes in situ by proximity ligation. *Nat. Methods*. 3:995–1000. http://dx.doi.org/10.1038/nmeth947

Sudakin, V., G.K. Chan, and T.J. Yen. 2001. Checkpoint inhibition of the APC/C in HeLa cells is mediated by a complex of BUBR1, BUB3, CDC20, and MAD2. *J. Cell Biol.* 154:925–936. http://dx.doi.org/10.1083/jcb.200102093

Tipton, A.R., M. Tipton, T. Yen, and S.T. Liu. 2011. Closed MAD2 (C-MAD2) is selectively incorporated into the mitotic checkpoint complex (MCC). *Cell Cycle*. 10:3740–3750. http://dx.doi.org/10.4161/cc.10.21.17919

Vinciguerra, P., N. Iglesias, J. Camblong, D. Zenklusen, and F. Stutz. 2005. Perinuclear Mlp proteins downregulate gene expression in response to a defect in mRNA export. *EMBO J.* 24:813–823. http://dx.doi.org/10.1038/sj.emboj.7600527

Vink, M., M. Simonetta, P. Transidico, K. Ferrari, M. Mapelli, A. De Antoni, L. Massimiliano, A. Ciliberto, M. Faretta, E.D. Salmon, and A. Musacchio. 2006. In vitro FRAP identifies the minimal requirements for Mad2 kinetochore dynamics. *Curr. Biol.* 16:755–766. http://dx.doi.org/10.1016/j.cub.2006.03.057

Washburn, M.P., D. Wolters, and J.R. Yates III. 2001. Large-scale analysis of the yeast proteome by multidimensional protein identification technology. *Nat. Biotechnol.* 19:242–247. http://dx.doi.org/10.1038/85686

Xu, X.M., A. Rose, S. Muthuswamy, S.Y. Jeong, S. Venkatakrishnan, Q. Zhao, and I. Meier. 2007. NUCLEAR PORE ANCHOR, the *Arabidopsis* homolog of Tpr/Mlp1/Mlp2/megator, is involved in mRNA export and SUMO homeostasis and affects diverse aspects of plant development. *Plant Cell*. 19:1537–1548. http://dx.doi.org/10.1105/tpc.106.049239

Zhao, X., C.Y. Wu, and G. Blobel. 2004. Mlp-dependent anchorage and stabilization of a desumoylating enzyme is required to prevent clonal lethality. *J. Cell Biol.* 167:605–611. http://dx.doi.org/10.1083/jcb.200405168